ELSEVIER

Journal of Alloys and Compounds 408–412 (2006) 687–692

Journal of ALLOYS AND COMPOUNDS

www.elsevier.com/locate/jallcom

# Electronic structure of rare-earth sesquioxides and oxysulfides

Masayoshi Mikami*, Shinichiro Nakamura

*Mitsubishi Chemical Group Science and Technology Research Center, Inc. 1000 Kamoshida-cho, Aoba-ku, Yokohama 227-8502, Japan*

Received 30 January 2004; received in revised form 13 December 2004; accepted 13 January 2005
Available online 6 July 2005

**Abstract**

Rare-earth sesquioxides $R_2O_3$ and oxysulfides $R_2O_2S$ (R = La, Ce, and Pr) have been theoretically investigated by first-principles pseudopotential method based on local density approximation in density functional theory. The structural, electronic, vibrational and dielectric properties of the rare-earth compounds are investigated with rare-earth pseudopotentials with 4f-electrons of rare-earth atoms as core states. Calculated properties related to the ground states appear consistent with the experimental results. The calculation result also indicates a possibility of another phonon mode assignment from Raman spectra of $La_2O_3$. The present work also implies that 4f-states are essential in electronic excitations to explain the variation of photo-absorption and body-color of $R_2O_3/R_2O_2S$.


*Keywords:* Insulators; Phosphors; Dielectric response; Electronic band structure; Phonon; Density functional theory; Luminescence; Rare-earth sesquioxide; Rare-earth oxysulfide

## 1. Introduction

Rare-earth (RE) sesquioxides $R_2O_3$ [1] and oxysulfides $R_2O_2S$ (R = Y and lanthanide) [2,3] are wide-gap materials that are attractive in technology viewpoint and are unique in scientific viewpoint. For the large RE ion (e.g. La, Ce, and Pr), the A-type structure of $R_2O_3$ belongs to the same space group with the structure of $R_2O_2S$, $D_{3d}^3$ ($P\bar{3}m1$); the only difference is that one of the three oxygen sites is occupied by a sulfur atom (Table 1). The primitive unit cell contains one molecule of $R_2O_3$ ($R_2O_2S$). The systems can be regarded as layered compounds. They have been investigated for phosphors, nano-structured materials for additive, coating, catalyst, and so forth. Recently $R_2O_3$ has been investigated for high-permittivity (high-*k*) materials, namely, alternative gate materials insulators [4]. It is thus crucial to understand the optical and dielectric properties of the RE systems for such practical applications.

Still, our understanding on the electronic structure of the systems appears lacking. For example, the variation of "band-gap" (detected by photo-absorption) of $R_2O_3$ has been known: 5.5 eV for $La_2O_3$, 2.4 eV for $Ce_2O_3$, 3.9 eV for $Pr_2O_3$ and so forth [5]. This trend has not been explained directly from the viewpoint of electronic structure. The body color variation of $R_2O_2S$ also suggests this kind of band-gap variation [3], although not all the band gaps of $R_2O_2S$ have been measured. However, only a few theoretical investigations have been conducted for the RE systems, only for the geometries and fundamental properties such as density of states [6–8]. Further, vibrational and dielectric properties of the RE systems are not fully understood from theoretical viewpoints.

The present work aims at theoretically evaluating structural, electronic, vibrational and dielectric properties of the RE systems. This study is expected for the quantitative understanding of the dielectric properties of $R_2O_3$ as the high-*k* candidates. Incidentally, the present authors have demonstrated a combination of such theoretical analysis and an empirical formula based on polaron, which leads to successful evaluation of the maximum scintillation efficiency in $Y_2O_2S$:Eu [9].

## 2. Calculation method

The present calculations have been performed owing to ABINIT code [10], which is based on first-principles pseudopotentials and plane waves in the framework of the density

* Corresponding author. Tel.: +81 459633834; fax: +81 459633835.
*E-mail address:* mikami.masayoshi@mv.m-kagaku.co.jp (M. Mikami).

0925-8388/$ – see front matter © 2005 Elsevier B.V. All rights reserved.
doi:10.1016/j.jallcom.2005.01.068

Table 1
Optimized structural parameters on $R_2O_2S$ and $R_2O_3$, along with experimental values with parentheses

| | $Y_2O_2S$ | $La_2O_2S$ | $Ce_2O_2S$ | $Pr_2O_2S$ | $La_2O_3$ | $Ce_2O_3$ | $Pr_2O_3$ |
|---|---|---|---|---|---|---|---|
| $a$ | 3.750 (3.791) | 4.035 (4.049) | 3.976 (4.008) | 3.930 (3.976) | 3.933 (3.940) | 3.871 (3.888) | 3.824 (3.859) |
| $c$ | 6.525 (6.596) | 6.914 (6.939) | 6.882 (6.886) | 6.752 (6.831) | 6.086 (6.130) | 6.001 (6.026) | 5.934 (6.013) |
| $c/a$ | 1.740 (1.740) | 1.714 (1.714) | 1.716 (1.718) | 1.718 (1.718) | 1.547 (1.556) | 1.550 (1.550) | 1.552 (1.558) |
| $u$ | 0.282 | 0.279 (0.279) | 0.280 | 0.281 | 0.247 (0.245) | 0.247 (0.245) | 0.247 (0.246) |
| $v$ | 0.631 | 0.629 (0.629) | 0.629 | 0.629 | 0.645 (0.645) | 0.645 (0.647) | 0.645 (0.656) |
| $B$ | 142 | 109 | 114 | 119 | 118 | 124 | 130 |

Lattice constants $a$ and $c$ in Å. Atom positions in $R_2O_2S$ ($R_2O_3$) using lattice vector unit are $\pm(1/3, 2/3, u)$ for 2$R$ with $u \approx 0.28(0.25)$, $\pm(1/3, 2/3, v)$ for 2O with $v \approx 0.63(0.65)$, and (0, 0, 0) for 1S (1O), respectively. Bulk modulus in GPa. Experimental data from Ref. [3] for $R_2O_2S$, Ref. [7] for $La_2O_3$, Ref. [8] for $Ce_2O_3$, and Ref. [32] for $Pr_2O_3$. The data for $Y_2O_2S$ come from the previous work [23]

functional formalism [11]. The exchange-correlation energy is evaluated within the local density approximation (LDA) by using Ceperley–Alder homogeneous electron gas data [12]. The wave functions are expanded in plane waves up to a kinetic-energy cutoff of 80 Hartree. Integrals over the Brillouin zone (BZ) are replaced by a sum on a Monkhorst–Pack grid of (4 × 4 × 2) special $k$-points [13]. The geometrical optimization are performed with Broyden–Fletcher–Goldfarb–Shanno minimization.

Troullier–Martins-type pseudopotentials, [14] generated thanks to the FHI98PP code, [15] have been adopted in this work. An important part of this work is the constructions of reliable pseudopotentials of the RE atoms. The electronic configuration of the RE atoms is taken as $[Kr]4d^{10}4f^x5s^25p^65d^15s^2$ ($x = 0, 1, 2$ for La, Ce, Pr, respectively). We treated the 5s, 5p, 5d, 6s electrons as valence states, while $[Kr]4d^{10}4f^x$ as core states; the cut-off radii for valence electron pseudo-wavefunctions are taken just before the outmost maximum of the corresponding true atomic-wavefunction [16]. Since our RE pseudopotentials are prepared to have good transferability for the ground state calculations, electronic excitation related to 4f-states are beyond the scope of the present study. Still, the present work is useful to see if the variation of the "energy gap" between the anion p-states and the RE d-states among $R_2O_3$ ($R_2O_2S$).

The phonon modes, dielectric permittivity tensors, and Born effective charge tensors are evaluated by the density functional perturbation theory (DFPT). [17] Technical details employed in the present computation of the second-order responses to atomic displacements and homogeneous electric fields can be found in Ref. [18], while Ref. [19] presents the subsequent computation of dynamical matrices, Born effective charges, dielectric permittivity tensors and so forth. The present authors have successfully applied the DFPT to several inorganic [9,20,21] and organic [22] systems.

## 3. Results and discussions

We first calculated the total energies of $R_2O_3$ and $R_2O_2S$ as a function of volume and found the equilibrium volumes by fitting the computed values to Murnaghan's equation of state. The calculated parameters (Table 1) agree well with the experimental data within about 1% errors, which are typical in LDA calculations. It is noted that the R–O/R–S bond lengths appear close to the sum of the corresponding Shannon's ionic radii. The atomic structure may thus be regarded as the result of ion-packing.

Fig. 1 shows the calculated band structures of $R_2O_3$ and $R_2O_2S$ at the optimized equilibrium volume. The results indicate that they have indirect gaps, although the band gaps are underestimated due to the LDA; the experimental (calculated) band-gaps are 5.5 eV [5] (3.6 eV) for $La_2O_3$, and 4.6 eV [23] (2.7 eV) for $La_2O_2S$, respectively. The topology of $R_2O_2S$ bandstructure appears similar with that of $Y_2O_2S$, [23] because of the present treatment of 4f-states as core electrons. Topology similarity between the bandstructure of $R_2O_2S$ and that of $R_2O_3$ can also be confirmed due to the similarity in the atomic geometries.

To identify the character of the conduction/valence bands, we focus on the density of states (DOS) of $La_2O_2S$ and $La_2O_3$. Fig. 2 shows the total DOS and atom-projected DOS of $La_2O_2S$ and $La_2O_3$. From the atom-projected DOS, the valence bands have the character of the p-states of the anions, whereas the conduction bands have the character of the La d-states. It is interesting to note that both the p-states of the anion at $\pm(1/3, 2/3, v)$ and the p-states of the anion at the origin cover all the valence bands in $La_2O_2S$ ($La_2O_3$) with the overlap with La d-states in complex manner. We thus expect some degree of covalency between the La atoms and the anions from the overlap in the atom-projected DOS for the both compounds, although it is practically difficult to perform band-by-band decomposition of the DOS. The topology difference in the bandstructure between $La_2O_2S$ and $La_2O_3$ causes the shape difference in the DOS, in particular, near the top of the valence bands.

We also note the wider bandwidth in the sequence from La to Pr (Fig. 1) by closer examination of the bandstructures of $R_2O_3$ ($R_2O_3$). This implies stronger covalency in this order. The strength of the covalency may be related to the calculation result of the cohesive (atomization) energies; 43.3 eV, 43.9 eV, 44.2 eV for $La_2O_3$, $Ce_2O_3$, $Pr_2O_3$, and 41.2 eV, 41.7 eV, 42.0 eV for $La_2O_2S$, $Ce_2O_2S$, $Pr_2O_2S$, respectively, although the LDA will overestimate the cohesive energies. This trend in the bond strength may also be related to the variation of the bulk moduli (Table 1) and the phonon

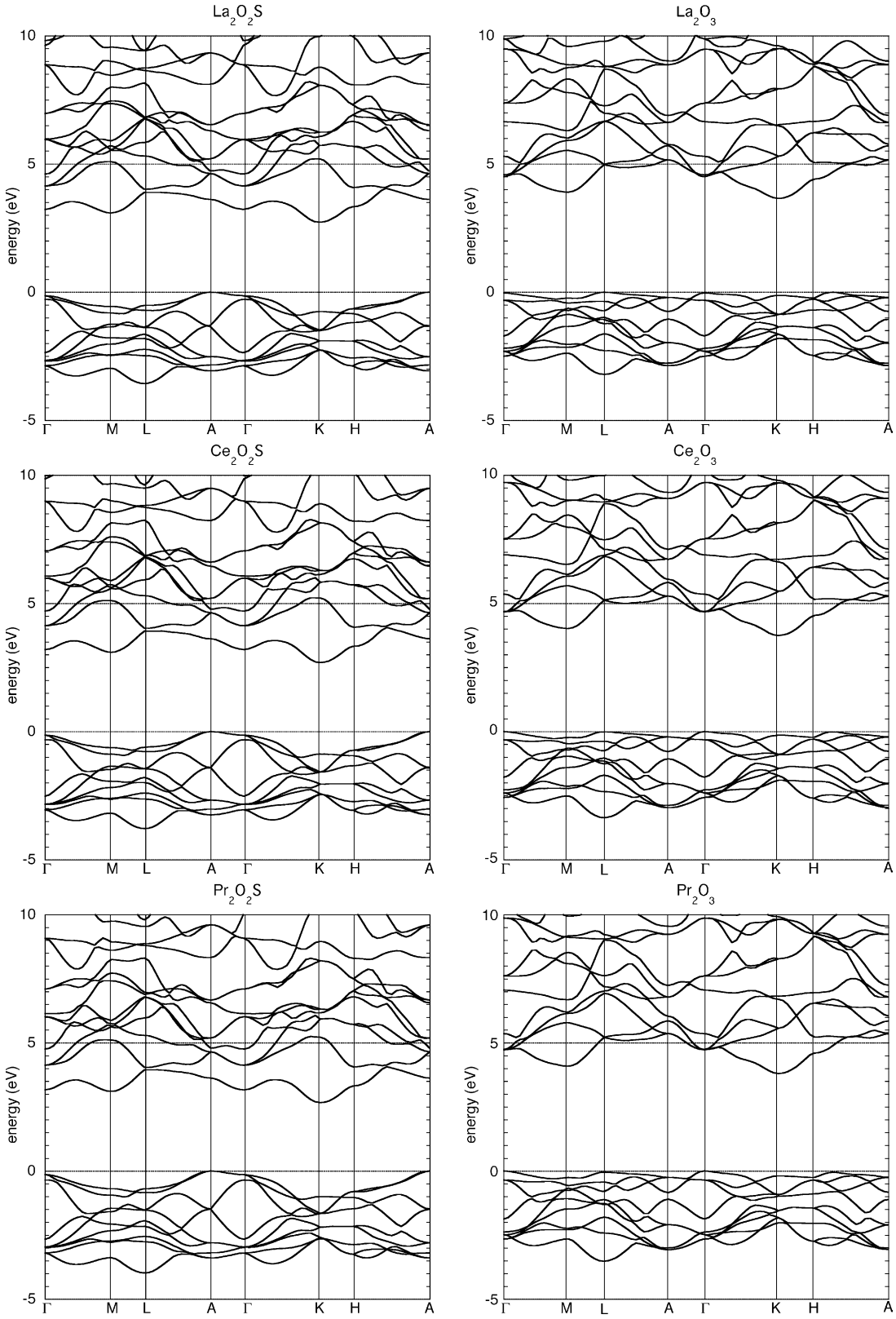


Fig. 1. Band structures of $R_2O_2S$ and $R_2O_3$ (R = La,Ce,Pr). The energies are relative to the top of valence bands (the anion p-states). The conduction bands consist of the RE d-states. Note that 4f-electrons of the R atoms are treated as core electrons, which should be somewhere in the conduction bands (for R = La) or in the energy gap between the anion p-states and the cation d-states (for R = Ce,Pr). The valence band widths of $R_2O_2S$ ($R_2O_3$) are 3.4, 3.6, and 3.8 eV (3.0, 3.1, 3.2 eV) for R = La, Ce, and Pr, respectively.

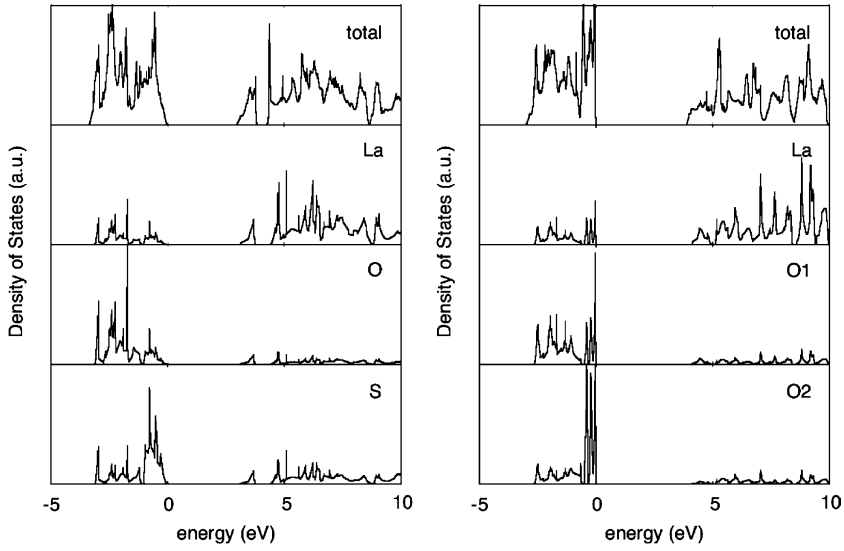


Fig. 2. Total and atom-projected density of states of $La_2O_2S$ (left) and $La_2O_3$ (right). O1 (O2) denotes the oxygen at $\pm(1/3, 2/3, v)$ with $v \approx 0.65$ (at the $(0, 0, 0)$) in $La_2O_3$.

wavenumbers, which we will see later (Table 2). Thus the above calculation results appear consistent.

Even though the LDA energy gap should be regarded as qualitative, little variation of the calculated energy gaps in $R_2O_3$ indicates that the variation of the experimental band-gaps in $R_2O_3$ cannot be expected in the band-structures without 4f-states. In fact, the photo-absorption can be ascribed to the local excitation in the RE atom involving 4f-states. Specifically, the absorption energies of $4f^{n-1}5d^1$ or charge transfer state (CTS) transition, given by Jørgensen [24], appears to explain the band-gap variation of $R_2O_3$. (See Fig. 25 on the page 184 of Ref. [2], which depicts the transition energies from the ground state to the $4f^{n-1}5d^1$/CTS of the RE dopants in $R_2O_3$). It is interesting to note that the variation of the 4f-state positions of the RE dopants has been clarified in some wide-gap materials by Dorenbos [25]; he also discusses the relation between the 4f-state in the energy gap and the $4f^{n-1}5d^1$/CTS transitions. From the above consideration, it appears natural to expect the similar bandgap variation of $R_2O_2S$ for the explanation of the variation of the body colors [3].

Next, the Raman/Infra-red(IR) phonon modes are theoretically evaluated (Table 2). The vibrational mode assignment is explained in our previous work on $Y_2O_2S$ [20]. Notice that the IR modes ($E_u$, $A_{2u}$) include the sulfur (oxygen) atom motion at the origin in the unit cell, whereas the Raman modes ($E_g$, $A_{1g}$) do not; the internal modes limited within the parallelogram of $R_2O_2$ are the Raman active. Thus we may expect that the Raman-active modes of $R_2O_2S$ have similar character with those of $R_2O_3$ to some degrees.

Table 2
Theoretical and experimental phonon mode wavenumbers (unit: $cm^{-1}$) of $R_2O_2S$ and $R_2O_3$ (R = La,Ce,and Pr)

| Mode | $Y_2O_2S$ | $La_2O_2S$ | | $Ce_2O_2S$ | | $Pr_2O_2S$ | | $La_2O_3$ | | $Ce_2O_3$ | $Pr_2O_3$ |
|---|---|---|---|---|---|---|---|---|---|---|---|
| | Theory | Theory | Experiment | Theory | Experiment | Theory | Experiment | Theory | Experiment | Theory | Theory |
| Raman | | | | | | | | | | | |
| $E_g$ | 142 | 107 | 104 | 109 | 106 | 111 | 101 | 106 | 74 | 108 | 110 |
| $A_{1g}$ | 259 | 201 | 196 | 203 | | 205 | 190 | 201 | 108 | 203 | 205 |
| $E_g$ | 493 | 383 | 360 | 394 | | 404 | 372 | 430 | 444 | 445 | 457 |
| $A_{1g}$ | 497 | 398 | 392 | 410 | 409 | 421 | 412 | 403 | 408 | 416 | 428 |
| Infrared | | | | | | | | | | | |
| $E_u$ | 201(TO) | 193(TO) | 262 | 197(TO) | 248 | 200(TO) | | 191(TO) | 242 | 198(TO) | 203(TO) |
| | 238(LO) | 223(LO) | 276 | 228(LO) | 282 | 231(LO) | | 299(LO) | | 308(LO) | 316(LO) |
| $A_{2u}$ | 264(TO) | 201(TO) | 212 | 237(TO) | 200 | 241(TO) | | 216(TO) | 242 | 227(TO) | 228(TO) |
| | 330(LO) | 297(LO) | | 303(LO) | | 308(LO) | | 397(LO) | | 408(LO) | 417(LO) |
| $E_u$ | 433(TO) | 333(TO) | 420 | 342(TO) | 417 | 349(TO) | | 397(TO) | 435 | 409(TO) | 418(TO) |
| | 565(LO) | 474(LO) | 458 | 483(LO) | 450 | 491(LO) | | 556(LO) | | 569(LO) | 580(LO) |
| $A_{2u}$ | 461(TO) | 406(TO) | 370 | 415(TO) | 348 | 423(TO) | | 440(TO) | 386 | 451(TO) | 460(TO) |
| | 586(LO) | 513(LO) | | 524(LO) | | 533(LO) | | 512(LO) | | 523(LO) | 539(LO) |

The symbol TO (LO) denotes transverse (longitudinal) optical mode. The experimental data come from Ref. [3] for $R_2O_2S$ and Ref. [27] for $La_2O_3$. As to the Raman experiment of $La_2O_3$, the observed mode of 192 $cm^{-1}$ was dimissed as the overtone of the mode of 108 $cm^{-1}$. The data of $Y_2O_2S$ come from Ref. [20]

Table 3
Born effective charge and high- and low-frequency dielectric permittivity tensor elements ($\epsilon^{\infty}$ and $\epsilon^{0}$) of $La_2O_2S$ and $La_2O_3$

| | $\alpha\alpha$ | $Z^*_{\alpha\alpha}$(La) | $Z^*_{\alpha\alpha}$(O) | $Z^*_{\alpha\alpha}$(S/O) | $\epsilon^{\infty}_{\alpha\alpha}$ | $\epsilon^{0}_{\alpha\alpha}$ | $\epsilon^{0}_{\alpha\alpha} - \epsilon^{\infty}_{\alpha\alpha}$ |
|---|---|---|---|---|---|---|---|
| $Y_2O_2S$ | *xx* | +3.66 | −2.53 | −2.28 | 5.23 (4.29) | 12.51 | 7.28 |
| | *zz* | +3.71 | −2.63 | −2.16 | 4.87 (4.07) | 12.20 | 7.33 |
| $La_2O_2S$ | *xx* | +3.95 | −2.78 | −2.34 | 5.45 (4.53) | 14.72 | 9.27 |
| | *zz* | +3.99 | −2.79 | −2.40 | 5.23 (4.40) | 13.80 | 8.57 |
| $Ce_2O_2S$ | *xx* | +3.94 | −2.78 | −2.33 | 5.49 | 14.67 | 9.18 |
| | *zz* | +3.98 | −2.79 | −2.37 | 5.25 | 13.71 | 8.46 |
| $Pr_2O_2S$ | *xx* | +3.92 | −2.76 | −2.31 | 5.51 | 14.58 | 9.07 |
| | *zz* | +3.96 | −2.79 | −2.35 | 5.24 | 13.63 | 8.39 |
| $La_2O_3$ | *xx* | +4.09 | −2.74 | −2.71 | 4.83 (4.13) | 23.20 | 18.37 |
| | *zz* | +3.78 | −2.49 | −2.57 | 4.69 (4.02) | 21.54 | 16.85 |
| $Ce_2O_3$ | *xx* | +4.08 | −2.73 | −2.69 | 4.82 | 22.65 | 17.83 |
| | *zz* | +3.76 | −2.48 | −2.56 | 4.67 | 21.07 | 16.40 |
| $Pr_2O_3$ | *xx* | +4.06 | −2.72 | −2.67 | 4.80 | 22.21 | 17.41 |
| | *zz* | +3.74 | −2.46 | −2.55 | 4.64 | 20.67 | 16.03 |

The theoretical prediction with the scissor correction technique are denoted in parentheses. The data of $Y_2O_2S$ come from Ref.[9]

In the phonon calculations of $R_2O_2S/R_2O_3$, Raman-active modes are well reproduced, while IR-active modes are not, at the first glance. Unfortunately, only a few IR experimental works performed in 1970s are available [26,27]. We suspect the accuracy of the experimental data, as discussed in Ref. [20] With respect to the discrepancy between theory and experiment in Raman vibrational modes of $La_2O_3$, it is noteworthy that the author of Ref. [27] reported a Raman mode of 192 $cm^{-1}$, which was dismissed as the overtone of the Raman mode of 108 $cm^{-1}$. Our calculation indicates that the observed mode of 192 $cm^{-1}$ may be one *fundamental* Raman active mode, while the mode of 74 $cm^{-1}$ may come from different sources. Our new mode assignment appears plausible in the light of the expected similarity in the Raman modes of $La_2O_2S$ and $La_2O_3$, as we stated before. If our assumption holds true, the agreement between theory and experiment can be well expected. Further investigations should be awaited to clarify this point.

The high- and low-frequency dielectric tensor components ($\epsilon^{\infty}$ and $\epsilon^{0}$) along the *a*- and *c*-axes are evaluated, along with the Born effective charge tensors (Table 3). Whereas $\epsilon^{\infty}$ originates from electronic polarization, the difference ($\epsilon^{0} - \epsilon^{\infty}$) originates from ionic polarization expressed by phonon modes and Born effective charges; this is the contribution from the IR phonon modes. The explicit equation can be found elsewhere [18,19]. Note that the calculated high-frequency dielectric constants for the Ce/Pr-compounds may not be physically meaningful due to resonance effect arising from photo-absorption involving 4f-states in the energy gap between the anion p-states and the RE 5d-states. The experimental high-frequency dielectric constant of $La_2O_2S$ ($La_2O_3$) may be estimated as 4.67 (3.63) from the square of the refractive index [28,29]. The calculated $\epsilon^{\infty}$ is overestimated due to the LDA; the agreement between theory and experiment can be somewhat achieved by adopting the scissor correction technique with the scissor parameter 1.9 eV to reproduce the experimental band gap of $R_2O_2S/R_2O_3$. The present result may indicate that the high-frequency dielectric constant of $R_2O_2S$ is larger than that of $R_2O_3$ due to the larger polarization of "electron cloud" around sulfur anion than around oxygen anion.

On the other hand, the low-frequency (static) dielectric tensor components of $La_2O_3$ are larger than those of $La_2O_2S$; the evaluated $\epsilon^{0}$ value of $La_2O_3$ appears typical in experiments of RE sesquioxides [4]. From the relationship among dielectric tensors and Born effective charge [19], the larger $\epsilon^{0}$ value in $La_2O_3$ than in $La_2O_2S$ can be ascribed to the larger Born ionic charge in oxygen than in sulfur anion at the origin. The Born effective charge depends on the electronic charge reorganization induced by virtual atomic displacement due to the definition as *dynamical* effective charge [30]. Thus, this difference between $\epsilon^{0}$ of $La_2O_3$ and $\epsilon^{0}$ of $La_2O_2S$ can be understood from the viewpoint of the electronegativity difference between oxygen and sulfur.

## 4. Conclusion

We have investigated structural, electronic, vibrational, and dielectric properties of $R_2O_3$ and $R_2O_2S$, from the standpoint of the first-principles calculation. The phonon modes, high-frequency and static dielectric tensors, and Born effective charge tensors are evaluated by the DFPT. The agreement between the theory and the experiments appears satisfactory, if we consider possible errors in experimental data and the present theoretical approximation. In particular, our calculation has pointed out another possibility on the Raman mode assignment of $La_2O_3$. Further experimental and theoretical studies are encouraged to confirm our theoretical predictions.

Although the structural, vibrational and dielectric properties have been well investigated, the photo-absorption in $R_2O_3/R_2O_2S$ cannot be discussed quantitatively in the present work, For this purpose, the RE 4f-states must be explicit included in ab initio calculations. At present we have to point out two major difficulties within the DFT formalism; underestimation of "energy gap" between anion p-states and RE 5d-states, and unreliable predictions of the position of the very localized 4f-states in the energy gap due to the

strong electron correlation. Accurate theoretical prediction of the position of the 4f-states in the corrected "energy gap" would lead to understanding not only the variation of photoabsorption of $R_2O_3/R_2O_2S$ but also other physical properties closely related to the RE trap levels [25]; for example, long-life phosphorenscence enabled by RE co-dopants, photocarrier generation (or luminescence) by Ce-doping [31], and so forth. Further progress in the DFT is thus awaited.

## References

[1] G. Adachi, N. Imanaka, Chem. Rev. 98 (1998) 1479.
[2] See, for, example, S. Shionoyan, W.M. Yen (Eds.), Phosphor Handbook, CRC Press, Boca Raton, FL, 1998.
[3] G. Czack, et al. in: G. Czack (Eds.), Gmelin Handbook of Inorganic Chemistry, Springer-Verlag, Berlin, 1983, p. 560 (Chapter 7).
[4] S. Ohmi, et al., J. Electrochem. Soc. 150 (2003) 134.
[5] A.V. Prokofiev, et al., J. Alloys Compd. 242 (1996) 41.
[6] N. Hirosaki, et al., J. Alloys Compd. 351 (2003) 31.
[7] Y.L. Page, et al., Acta Cryst. B 58 (2002) 349.
[8] N.V. Skorodumova, et al., Phys. Rev. B 64 (2001) 115108.
[9] M. Mikami, J. Lumin. 102–103 (2003) 7.
[10] The ABINIT code is a common project of the Université Catholique de Louvain, Corning Incorporated, and other contributors. http://www.abinit.org/the Université de Liegè, the Commissariat a l'Energie Atomique, Mitsubishi Chemical Corporation, and other contributors; X. Gonze, et al., Comput. Mater. Sci. 25 (2002) 478.
[11] R.M. Martin, Electronic Structure: Basic Theory and Practical Methods, Cambridge University Press, 2004.
[12] D.M. Ceperley, B.J. Alder, Phys. Rev. Lett. 45 (1980) 566.
[13] H.J. Monkhorst, J.D. Pack, Phys. Rev. B 13 (1976) 5188.
[14] N. Troullier, J.L. Martins, Phys. Rev. B 43 (1991) 1993.
[15] M. Fuchs, M. Scheffler, Comput. Phys. Commun. 119 (1999) 67.
[16] N. Richard, S. Bernard, J. Alloys Compd. 323–324 (2001) 628.
[17] S. Baroni, Rev. Mod. Phys. 73 (2001) 515.
[18] X. Gonze, Phys. Rev. B 55 10 (1997) 337.
[19] X. Gonze, C. Lee, Phys. Rev. B 55 10 (1997) 355.
[20] M. Mikami, et al., Phys. Rev. B 65 (2002) 094302.
[21] M. Mikami, et al., Phys. Rev. B 66 (2002) 155213.
[22] M. Mikami, S. Nakamura, Phys. Rev. B 69 (2004) 134205.
[23] M. Mikami, A. Oshiyama, Phys. Rev. B 57 (1998) 8939.
[24] C.K. Jørgensen, et al., Z. Naturforschg 20a (1964) 54.
[25] P. Dorenbos, J. Phys.: Condens. Matter 15 (2003) 8417.
[26] Yu.M. Golovin, et al., J. Appl. Spectrosc. [USSR] 18 (1973) 62.
[27] J.H. Denning, S.D. Ross, J. Phys. C 5 (1972) 1123.
[28] L.E. Sobon, et al., J. Appl. Phys. 42 (1971) 3049.
[29] Y.Y. Guo, et al., Solid State Ionics 123 (1999) 225.
[30] Ph. Ghosez, et al., Phys. Rev. B 58 (1998) 6224.
[31] W.M. Yen, et al., J. Lumin. 69 (1996) 287.
[32] O. Greis, et al., J. Alloys Compd. 216 (1994) 255.